

Polarizable Particle Aggregation Under Rotating Magnetic Fields Using Scattering Dichroism

Sonia Melle,^{*,†} Oscar G. Calderón,[‡] Gerald G. Fuller,^{*,1} and Miguel A. Rubio[†]

^{*}Department of Chemical Engineering, Stanford University, Stanford, California 94305-5025; [†]Dpt. Física Fundamental, UNED. Av. Senda del Rey 9, Madrid 28040, Spain; and [‡]Dpt. Optica, Universidad Complutense de Madrid, Ciudad Universitaria, Madrid 28040, Spain

Received March 15, 2001; accepted November 8, 2001; published online January 10, 2002

We used scattering dichroism to study the dynamics of dipolar chains induced in magnetorheological suspensions under rotating magnetic fields. Both the dichroism (proportional to the total number of aggregated particles) and the phase lag show different behavior below and above a cross-over frequency. The cross-over frequency depends linearly on both the square of the magnetization and the inverse of the viscosity. The Mason number (ratio of viscous to magnetic forces) governs the dynamics. Therefore, there is a cross-over Mason number below which the dichroism remains almost constant and above which the rotation of the field prevents the particle aggregation process from taking place. Our experimental results have been compared with particle dynamics simulations showing good agreement. © 2002 Elsevier Science (USA)

Key Words: magnetorheological suspensions; rotating fields; scattering dichroism.

1. INTRODUCTION

Magnetorheological (MR) suspensions consist of magnetizable particles suspended in a nonmagnetic fluid. The wide range of technological applications of these suspensions has excited considerable interest concerning the relationship between microscopic structure and mechanical and optical properties of these systems. Moreover, they are also a good model system for the study of structure formation and dynamics in suspensions with tunable interaction between dipolar particles. It is well known that when a unidirectional magnetic field is applied, the particles in the suspension acquire a dipole moment $\mathbf{m} = (4\pi/3)a^3\mathbf{M}$, where \mathbf{M} and a are the particle magnetization and diameter, respectively. Due to dipolar interactions, these particles join to form chain structures in the field direction inducing an optical anisotropy in the sample due to polarization dependent scattering from oriented aggregates. When the size of the scattering object is comparable to the wavelength of the light (λ_i), the induced dichroism will be bigger than the induced birefringence (1, 2). Scattering dichroism has been shown (3, 4) to be a good technique for the study of these anisotropic struc-

tures in MR suspensions at moderate concentration which cannot be readily studied with other optical techniques, such as videomicroscopy.

The dynamics of MR suspensions under rotating magnetic fields has been studied recently (3). We found that the field-induced chains rotate synchronously with the field but lag behind by a constant phase angle. Previous experimental work on magnetic holes (5) and liquid crystals (6, 7) under rotating magnetic fields has explored the dynamics of such systems depending on the value of the driving frequency. It has been shown previously, with both scattering dichroism (3) and videomicroscopy experiments (8), that MR suspensions have the capacity of reducing the size of the structures to decrease their viscous drag while rotating synchronously with the field (9). Furthermore, within this synchronous regime, two different behaviors were found below or above a cross-over frequency, f_c . Below f_c , the dichroism remains almost constant and the phase lag increases quasi-linearly. However, above f_c , the dichroism decreases (3) following a power law with an exponent -1 , while the increase of the phase lag is relatively slow. The cross-over frequency was found to increase with the amplitude of the applied field.

In this paper we analyze the interplay between magnetic and viscous forces over the cross-over frequency separating these two regimes. We have studied the dependence of the cross-over frequency on the magnetization by applying magnetic fields with different amplitudes on the same suspension. The dependence of the cross-over frequency on the viscosity of the carrier fluid was analyzed applying a rotating field of constant amplitude on suspensions with different glycerol concentrations.

A dimensionless parameter that compares magnetic and viscous forces is the well-known Mason number. This number has been defined with different proportionality factors in the literature (10–12). The Stokes viscous force acting on two particles in contact which rotate with a field of frequency ω is $F_h \sim 6\pi\eta a(\omega a)$, where η is the solvent viscosity. The dipolar magnetic force is $F_m \sim (\pi/2)\mu_0 a^2 M^2$, where μ_0 is the vacuum magnetic permeability. Then, the Mason number is given by:

$$\text{Ma} = \frac{12^2 \eta \omega}{\mu_0 M^2}, \quad [1]$$

¹ To whom correspondence should be addressed. Fax: (650) 725-7294. E-mail: ggf@chemeng.stanford.edu.

where the proportionality factor has been chosen to be in agreement with the dimensionless frequency obtained from the theoretical analysis (section 3.2).

We found that the cross-over frequency separating the two regimes increases linearly with the square of the magnetization and decreases with the inverse of the viscosity, so the Mason number governs the dynamics of field-induced dipolar chains under rotating fields. As expected from this result, we obtained a good collapse of the dichroism and the phase lag curves (measured at different magnetic fields and viscosities) with Mason number. The change in behavior of the dichroism and the phase lag occurs at a cross-over Mason number, $Ma_c \approx 1$, above which the viscous forces dominate and inhibit the aggregation process. We corroborated our experimental findings through the results obtained from particle dynamics simulations. The simulations show that the average length of the chains decreases with frequency following a power law with an exponent close to -0.5 . Furthermore, the simulations also reveal that the whole scenario, i.e., the two different behaviors for the total number of aggregated particles and the phase lag above and below the cross-over frequency, is in good agreement with the experiments.

2. MATERIALS AND METHODS

2.1. MR Suspensions and Procedure

We prepared glycerol suspensions at different concentrations using two water suspensions of polystyrene (PS) polydisperse microspheres loaded with iron oxide grains. The aqueous suspensions (M1-180/12 and M1-070/60) were bought from Estapor-Rhône Poulenc with a solid content of 10% by weight. The particle properties are listed in Table 1. The surface of these microspheres is composed of carboxylic acid ($-\text{COOH}$) groups with an added surfactant coating layer of sodium dodecyl sulfate (SDS) to stabilize the suspensions. Since these small magnetite grains are randomly oriented inside the microparticles, the resulting magnetic moment is zero in the absence of an external magnetic field. Under sufficiently low magnetic fields these particles exhibit superparamagnetic behavior with virtually no hysteresis or magnetic remanence as a result of the orientation of the magnetite grains dispersed in the PS matrix.

Two experimental procedures were used and are summarized in Table 2. To study the effect of the magnetic forces on the cross-over frequency, we diluted the suspension of particles of

TABLE 2

Summary of the Experimental Conditions

Experimental parameters	Magnetic field effect	Influence of viscosity
Suspension	d-M1-180/12	d-M1-070/60
Glycerol volume content	82.5%	40–80%
Volume fraction	$\phi = 0.016$	$\phi = 0.01$
Field strength (kA/m)	$H = 6.2\text{--}24.8$	$H = 3.1$

diameter $1.01 \mu\text{m}$ (M1-180/12) in glycerol to achieve a solvent volume concentration of 82.5% glycerol with a volume fraction of $\phi = 0.016$. We will denote the resulting suspension as d-M1-180/12 hereafter. The dilution in glycerol reduced the SDS concentration and additional SDS was added to achieve a concentration equal to the original solution (5 g/L). The viscosity of the suspension d-M1-180/12 was measured without applying a magnetic field using a Rheometrics Dynamic Analyzer RDA II to be $\eta = (0.178 \pm 0.002) \text{ Pa s}$ at 10°C . The first set of experiments consists on applying rotating magnetic fields with different amplitudes (ranging from $H = 6.2 \text{ kA/m}$ to $H = 24.8 \text{ kA/m}$) on suspension d-M1-180/12. For high fields, the dipole moment induced on the particles is not directly proportional to the applied field. To determine this nonlinear response, we measured the particle magnetization curve with a LakeShore 7300 vibrating sample magnetometer (VSM) for the range of magnetic fields used in the experiments. The result is shown in Fig. 1. As expected, the particles show a superparamagnetic behavior with no hysteresis but saturation effects in the magnetization at high field amplitudes appear.

For the second set of experiments we prepared suspensions with volume fraction $\phi = 0.01$ but different glycerol concentrations ranging from 40 to 80% in volume. In this case, we used the water suspension M1-070/60 with particles of $0.90 \mu\text{m}$ diameter. These suspensions are denoted as d-M1-070/60. We also determined their viscosities with the RDA II. The effect of the viscous force on the cross-over frequency was studied by applying a rotating magnetic field of constant amplitude

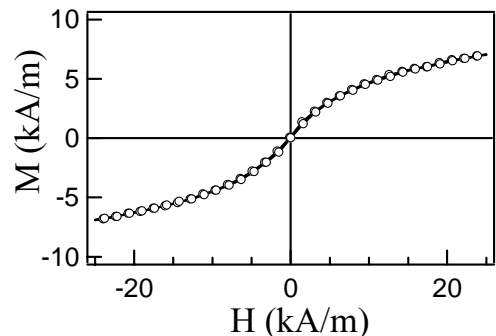


FIG. 1. Measured magnetization curve for the particles M1-180/12 in the range of magnetic fields reported in the experiments. The particles show a superparamagnetic behavior with no hysteresis but with saturation effects for high fields.

TABLE 1
Properties of the Magnetic Latex Microspheres Used

Particle properties	M1-180/12	M1-070/60
Mean diameter	$1.01 \mu\text{m}$	$0.90 \mu\text{m}$
Magnetic content	13%	62%
Saturation field	11.1 emu/g	52.7 emu/g
Surface group content	$20 \mu\text{eq/g}$	$145 \mu\text{eq/g}$

$H = 3.1$ kA/m on the suspensions d-M1-070/60. At such low magnetic field the magnetization varies approximately linearly with the field $\mathbf{M} = \chi_{\text{eff}}\mathbf{H}$, the effective magnetic susceptibility of the particle being $\chi_{\text{eff}} = 3(\mu_p - \mu_s)/(\mu_p + 2\mu_s) = 0.88$. Here μ_p and μ_s are the permeability of the particles and the solvent, respectively (14).

2.2. Experimental Setup

We have used scattering dichroism to study the dynamics of moderately concentrated magnetic dipolar suspensions (in the range of 1 to 2% in volume) under rotating magnetic fields. A full description of this experimental technique can be found in Refs. (3, 13). A schematic diagram of the optical train used to measure linear dichroism is shown in Fig. 2a and consists on a He-Ne laser, a polarizer (that sets the reference angle for the polarization), a photoelastic modulator, and a quarter wave plate (set at $\pi/4$ and null angular displacement with respect to the polarizer, respectively). The laser beam traverses the sample cell and the transmitted light is detected by a photodiode. The signal from the photodiode is sent to two phase lock-in amplifiers (Princeton Applied Research, EG&G-128A) and then digitized using a 16-bit resolution A/D data acquisition board (National Instruments, PCI-MIO-16xE-10). With this optical setup we can simultaneously measure the time evolution of the dichroism $\Delta n'' = n''_1 - n''_2$, i.e., the difference between the extinction of the incident light with polarization parallel and perpendicular to the long axis of the aggregates, and the orientation angle θ'' , i.e., the angle between the reference angle of the optical train and the long axis of the aggregates (see Fig. 2b). By comparing θ'' with the temporal evolution of the magnetic field

direction, given by ωt , we may define the phase lag between the field and the aggregates as $\alpha(t) = \omega t - \theta''(t)$.

The rotating magnetic field was achieved by applying sinusoidal electric signals to two orthogonal pairs of coils by means of two Kepco BOP20-10M power amplifiers, driven by two HP-FG3325A function generators referenced to one another at a phase difference of 90° . In Fig. 2c we show a sketch of the coils system as seen from the direction of the laser beam. The function generators allowed for control of both the amplitude and the frequency of the rotating magnetic field. These coils are embedded in a temperature-controlled aluminum cylinder to prevent heating effects. The suspension is placed between two quartz windows held in place by a Delrin attachment so that the separation between the windows is $e = 100 \mu\text{m}$ (see detail of the sample cell on Fig. 2d). All experiments were performed at a temperature of $T = 282 \pm 1$ K measured on the sample.

3. RESULTS AND DISCUSSION

3.1. Experimental Results

When a rotating field in the plane (X, Y) perpendicular to the optical path direction (axis Z) is applied, previous studies (8) show that particle chains continuously aggregate and fragment, although after a transient the ensemble achieves a steady-state chain size distribution. In the following figures we plot the dichroism and phase lag reached at the steady state, denoted as $\Delta n''_0$ and α_0 , respectively.

3.1.1. Magnetic field effect. In Fig. 3a the dichroism generated by the suspension d-M1-180/12 (82.5% glycerol, $\phi = 0.016$) is plotted versus the magnetic field frequency ($f = \omega/2\pi$) in a log-log form for various magnetic field strengths ($H = 6.2\text{--}24.8$ kA/m). As the frequency of the applied field is increased, the dichroism is reduced but not with the same rate. This plot clearly shows two distinct regions for frequencies below and above a cross-over frequency, f_c . Below this cross-over frequency, the dichroism is essentially independent of frequency. However, once this frequency is surpassed, the dichroism strongly decreases with frequency. Above 1 Hz, the dichroism drops with frequency with a scaling of approximately $\Delta n''_0 \simeq f^{-1}$. For high fields, the change in behavior is moved to higher frequencies, i.e., the cross-over frequency separating these two regions increases with the amplitude of the applied magnetic field. At higher fields the particle chains are more able to rotate with higher frequency fields. Since the strength of the interparticle magnetic forces scales with the square of the particle magnetization that dependence is also expected for the cross-over frequency. To test this dependence, $f_c \sim M^2$, we plot the dichroism curves obtained for different magnetic field strengths versus Ma number in Fig. 3b; it can be observed that the curves collapse onto a master curve.

The phase difference between the orientation of the aggregates and the magnetic field, α_0 , versus the frequency of the applied field is plotted in Fig. 4a for different field strengths. We observe that this phase lag increases with frequency over

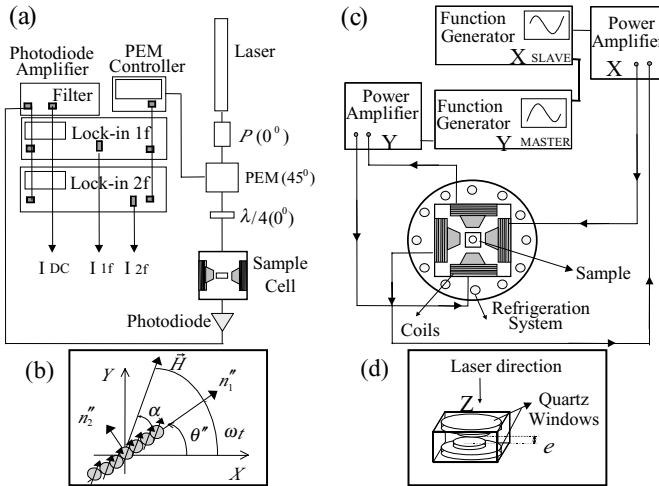


FIG. 2. Experimental setup. (a) Schematic diagram of linear dichroism optical train which enables one to measure the dichroism, $\Delta n'' = n''_1 - n''_2$, and the orientation angle of the structures, θ'' . (b) Definition of the phase lag, $\alpha(t) = \omega t - \theta''(t)$, between the magnetic field and the chains. (c) Sketch of the coils system to generate the rotating magnetic field. (d) Detail of the quartz cell filled with MR suspension.

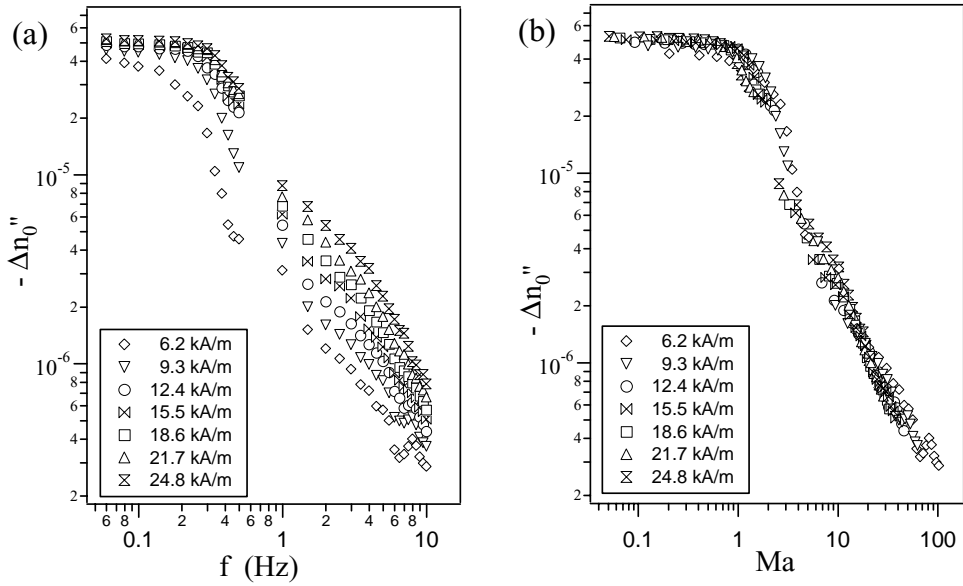


FIG. 3. Variation of the steady dichroism with rotational frequency (a) and collapse of dichroism with Ma number (b) for different magnetic field strengths in a log-log plot. Measurements for suspension d-M1-180/12 (82.5% glycerol content, $\phi = 0.016$). Power law fit with an exponent -1 for $Ma > Ma_c$.

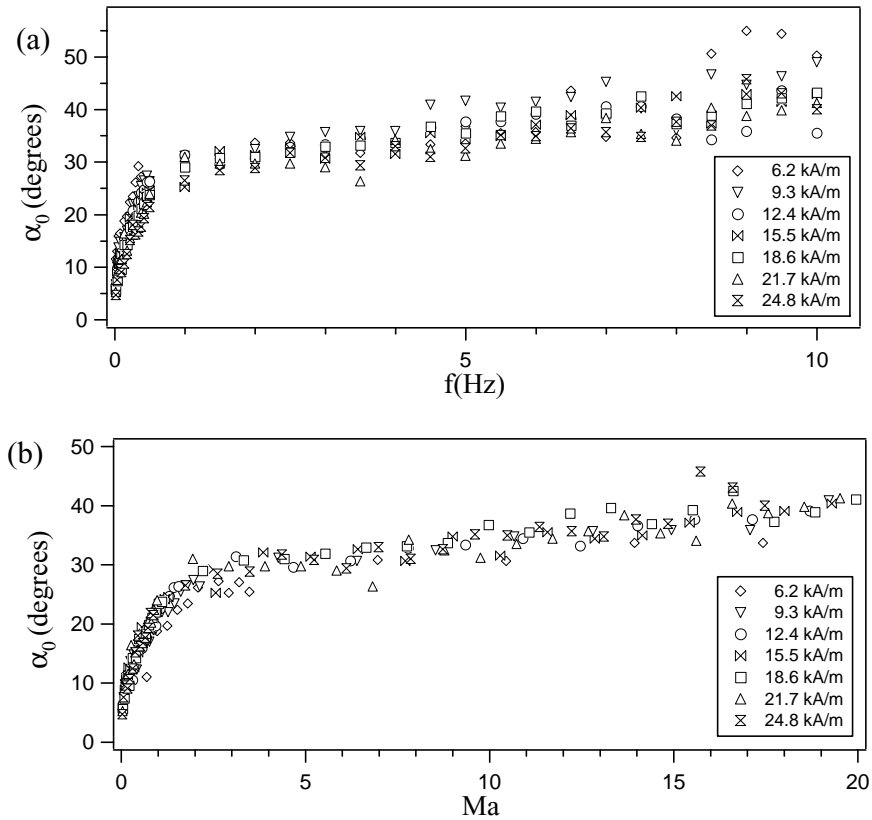


FIG. 4. Variation of the steady phase lag with rotational frequency (a) and collapse of the phase lag with Ma number (b) for different magnetic field strengths. Measurements for suspension d-M1-180/12 (82.5% glycerol content, $\phi = 0.016$).

the whole range of frequencies. However, as we found for the dichroism results, two different responses are observed, depending on the magnitude of the frequency. At low frequencies (below f_c) the phase difference grows very quickly while at high frequencies the increase of the phase lag is relatively slow. For frequencies larger than the cross-over frequency, the chains start to disappear so the contribution to the total average phase lag is due to the few small chains that still remain. These small chains lag behind the magnetic field with larger phase angles since they are close to breaking apart. In addition, a decrease of the phase lag with magnetic field intensity is observed. This behavior is expected since the angular component of the magnetic force, which is the responsible for the rotation of the chain, increases with the amplitude of the magnetic field. These data are replotted versus Ma number in Fig. 4b and, again, all curves nicely collapse onto a single master curve.

3.1.2. Influence of viscosity. To analyze the influence of the viscosity of the suspending medium, we measured the dichroism induced in the suspensions d-M1-070/60 (with different glycerol concentrations and the same particle volume fraction, $\phi = 0.01$) when a rotating field of amplitude $H = 3.1$ kA/m is applied. In Fig. 5a we plot the variation of the dichroism with rotational frequency in a log-log form for solutions with glycerol content ranging from 40 to 80%. Again, two different regimes above or below a cross-over frequency are observed. As expected, the cross-over frequency moves to bigger frequencies for low-viscosity suspensions because the structures are more free to rotate synchronously with the field. The collapse of those curves with Mason number is presented in Fig. 5b verifying the dependence of the cross-over frequency with the inverse of the viscosity, $f_c \sim \eta^{-1}$. Note that for low frequencies,

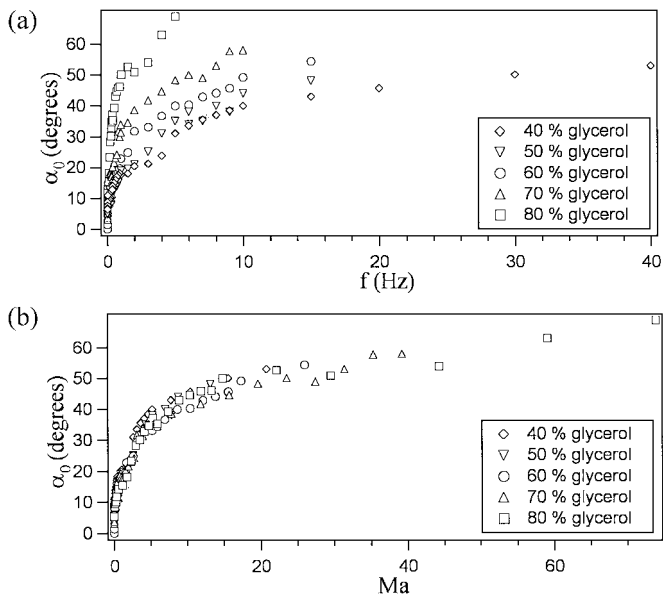
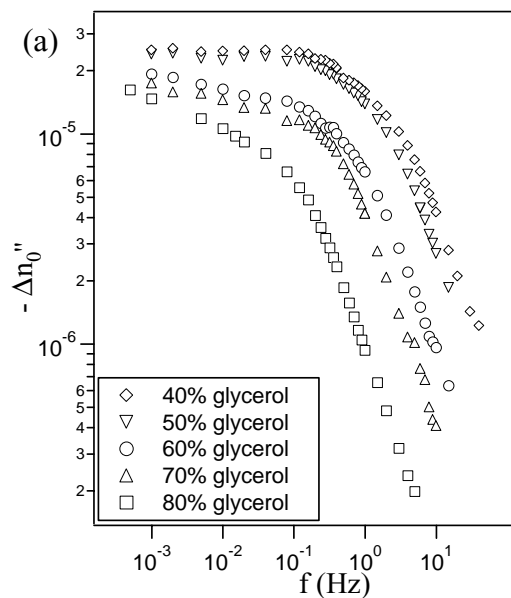


FIG. 6. Variation of the steady phase lag with rotational frequency (a) and collapse of the phase lag with Ma number (b) for suspensions d-M1-070/60 (different glycerol content, $\phi = 0.01$) in a log-log plot when a magnetic field of amplitude $H = 3.1$ kA/m is applied.

$f < f_c$, the dichroism shows a flatter plateau for solutions with less glycerol content (40–50%) which may be due to the fact that more viscous solutions need more time to reach the steady state.

The steady phase lag measured for these suspensions is plotted in Fig. 6a versus rotational frequency. We observe that the phase lag variation with the viscosity is much larger than the

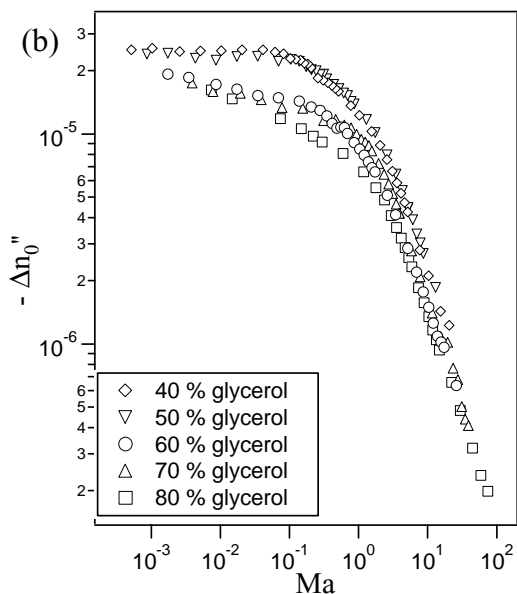


FIG. 5. Variation of the steady dichroism with rotational frequency (a) and collapse of dichroism with Ma number (b) for suspensions d-M1-070/60 (different glycerol content, $\phi = 0.01$) in a log-log plot when a magnetic field of amplitude $H = 3.1$ kA/m is applied.

variation encountered with field strength. As expected, more viscous suspensions show bigger phase lags. The collapse of those curves with Mason number is plotted in Fig. 6b.

These results emphasize the importance of the Mason number in controlling the aggregation phenomena in suspensions of polarizable particles in rotating magnetic fields. The change in behavior for both the dichroism and the phase lag corresponds to $\text{Ma}_c \approx 1$ when the viscous forces begin to overcome the magnetic forces.

3.2. Simulations

3.2.1. Equations of motion. Athermal particle dynamics simulations were conducted that consider the aggregation kinetics of N dipolar particles of diameter $2a$ suspended in a fluid of viscosity η and subjected to rotating magnetic fields of amplitude H and angular frequency ω . Taking into account that the aggregation takes place in the plane of the magnetic field rotation (15), we simplified our calculation by developing 2D simulations in this plane. Two fundamental length scales characterize the formation of chains. The first one is the so-called “thermomagnetic distance,” R_1 , which is the distance at which the magnetic energy corresponding to the dipolar interaction between two particles aligned in the field direction and with parallel dipole moments equals the thermal fluctuation energy. This length scale turns out to be $R_1 = 2a\lambda^{1/3}$, where λ is a dimensionless parameter calculated as the ratio between magnetic and thermal energies,

$$\lambda = \frac{\pi \mu_0 a^3 M^2}{9k_B T}, \quad [2]$$

where μ_0 is the vacuum magnetic permeability, and k_B is the Boltzmann constant. The physical meaning of R_1 is that particles that are separated by a distance larger than R_1 do not feel the magnetic interaction due to each other, because the energy of thermal fluctuations is larger than the dipolar interaction energy. The second length scale is the average initial interparticle distance, which can be estimated as $R_0 \simeq 2a/\phi^{1/3}$. Actually, the values of λ that correspond to the results reported here are $181 < \lambda < 712$ for the experiments with the suspension d-M1-180/12 and $\lambda = 322$ for the experiments with suspensions d-M1-070/60. Therefore, in these experiments, the magnetic energy is much higher than the thermal energy, and, since $R_1 > R_0$, the application of an external field H will immediately trigger the magnetic aggregation process. Consequently, we can safely neglect the effect of the Brownian motion on the evolution of the structures. As a first approximation, we will neglect higher order hydrodynamic interaction, and we will consider viscous forces to be represented as a Stokes force acting on each particle. Then, the equations of motion for the i th particle will contain the sum of the following three forces (16):

$$m \frac{d\mathbf{v}_i}{dt} = \mathbf{F}_h(\mathbf{v}_i) + \sum_{j \neq i} \mathbf{F}_d(\mathbf{r}_{ij}) + \sum_{j \neq i} \mathbf{F}_r(r_{ij}), \quad [3]$$

where $\mathbf{F}_h(\mathbf{v}_i) = -\gamma \mathbf{v}_i = -6\pi\eta a \mathbf{v}_i$ is the hydrodynamic Stokes force and \mathbf{v}_i is the particle velocity. The dipolar force over particle i th will be the sum of the dipole–dipole forces exerted by all the other particles. The dipole–dipole force between particles i th and j th is given by

$$\mathbf{F}_d(\mathbf{r}_{ij}) = \frac{3\mu_0 m^2}{4\pi r_{ij}^4} \{ [1 - 5(\hat{\mathbf{m}} \cdot \hat{\mathbf{r}}_{ij})^2] \hat{\mathbf{r}}_{ij} + 2(\hat{\mathbf{m}} \cdot \hat{\mathbf{r}}_{ij}) \hat{\mathbf{m}} \}, \quad [4]$$

where \mathbf{r}_{ij} is the separation vector between the two centers of mass, and we take \mathbf{m} to be aligned with the field direction. Note that as we are using one-particle Stokes’ hydrodynamics, a repulsive force, \mathbf{F}_r , must be included to avoid particles from overlapping. This force is calculated from (17)

$$\mathbf{F}_r(r_{ij}) = A \frac{3\mu_0 m^2}{4\pi (2a)^4} \exp[-B(r_{ij}/(2a) - 1)] \hat{\mathbf{r}}_{ij}, \quad [5]$$

where we set $A = 2$ and $B = 10$, so that for two particles that are in mechanical contact the repulsive force exactly balances the attractive dipolar magnetic interaction. Similar repulsive forces have been used in previous works (16, 17). Very simple order of magnitude calculations show that for the systems here studied, the inertial term in Eq. [3] can be discarded because the viscous drag term dominates. As usual (16, 18, 19), we can make the particle evolution Eq. [3] dimensionless, using the particle diameter, $2a$, as length scale, so that $r' = r/(2a)$, and a time scale $\tau = 12^2 \eta / (\mu_0 M^2)$, such that $t' = t/\tau$. Making these substitutions in Eq. [3], and dropping out the primes for simplicity, we arrive at

$$\frac{d\mathbf{r}_i}{dt} = \frac{\tau}{2a\gamma} \left[\sum_{j \neq i} \mathbf{F}_d(\mathbf{r}_{ij}) + \sum_{j \neq i} \mathbf{F}_r(r_{ij}) \right]. \quad [6]$$

This temporal scale leads to a dimensionless rotation frequency equal to $\Omega \equiv \omega\tau$. This dimensionless frequency is the well-known Mason number with the definition used in Eq. [1], $\Omega \equiv \text{Ma}$.

3.2.2. Simulation procedure. According to the preceding analysis, changing the field amplitude or the solvent’s viscosity, both account for a change in Ma . Therefore, in the simulations we have used only the Mason number as control parameter. The physical parameters used in the simulations reported here correspond to the suspension d-M1-180/12. The simulations being 2D, we have set the initial average interparticle distance so that it corresponds to the volume fraction in the experiment with that suspensions, $\phi = 0.016$, i.e., $R_0/(2a) \simeq 3.55$.

The numerical integrations have been performed using a time step of 0.005, which has proved to be small enough to avoid significant overlapping errors when the particles come into close contact. In all of the simulations the number of particles is 400, and the simulations are carried out in a square box of the proper size to adjust the initial average interparticle distance. The

particles are set initially at random positions avoiding overlapping, and all of the results here reported are statistical averages over different realizations corresponding to different initial spatial distributions of the particles. Each simulation is run long enough for the steady state to be reached and then the quantities to be compared with the experimental results are averaged during the last period of rotation of the field.

The comparison between experimental and simulation results deserves some comments. First, the chains are recognized by means of a criterion according to which two particles are aggregated when the distance between their respective centers of mass is smaller than 1.1 times the particle diameter. We have computed the dimensionless average chain length (average number of particles in a chain), L , in the usual way, i.e., if a chain labelled as j is formed by N_j particles, then

$$L = \frac{\sum_j N_j}{\sum_j 1}. \quad [7]$$

Mie's theory for light scattering by nonspherical objects allows us (4) to estimate the scattering dichroism generated from a chain j formed by N_j particles in the forward direction ($\varphi = 0$). Assuming that the chains can be approximated as cylindrical objects of radius a (2),

$$\Delta n''_j = \frac{2N_j}{k^2} (\text{Re}[T_2(\varphi = 0)] - \text{Re}[T_1(\varphi = 0)]), \quad [8]$$

where $k = 2\pi/\lambda_1$ is the wave vector of the laser beam and $T_i(\varphi = 0)$ is a function of k , a , and the isotropic refractive indexes of solvent and particles. In the case of a nonrotating field, all the chains are aligned in the same direction, and, assuming that the scattering dichroism produced from a set of N_c chains is the incoherent sum of the scattering dichroism produced by each chain, the total dichroism is proportional to the total number of aggregated particles N_a :

$$\Delta n'' = \sum_{j=1}^{N_c} \Delta n''_j \propto \sum_{j=1}^{N_c} N_j \equiv N_a. \quad [9]$$

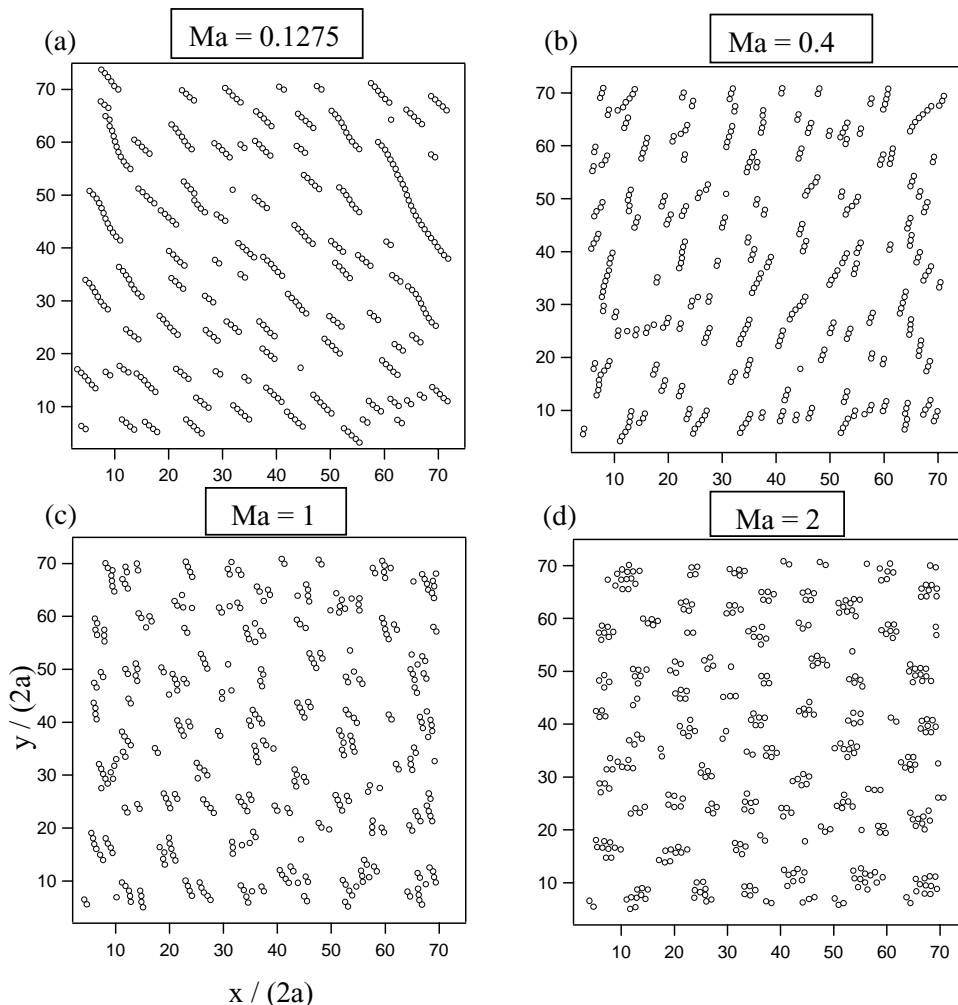


FIG. 7. Dimensionless particle positions for different dimensionless rotating frequencies, $\Omega \equiv \text{Ma}$, at an arbitrary time. Calculations for suspension d-M1-180/12 (82.5% glycerol content, $\phi = 0.016$).

In the case of rotating fields, chains of different length might lag behind the field with different phase angles. However, both videomicroscopy experiments (8) and the simulation results reported below show that the chain phase lag distribution is quite narrow, provided that the rotation frequency is not much larger than f_c . Therefore, in the following, we can safely presume that, for the measurements reported here, the dichroism will remain proportional to the total number of aggregated particles, N_a . Hence, we will compare the experimental value of the scattering dichroism with the value of N_a obtained in the simulations computed as

$$N_a \equiv \sum_j N_j, \quad [10]$$

where the sum is done for j with $N_j > 1$.

The phase lag of a given chain is the angular difference between the orientation of the magnetic field and the unit vector parallel to the long axis of the chain. For quasi-linear chains, we have determined the chain orientation vector by calculating the eigenvalues of the chains's inertia tensor, I_j^{\max} , I_j^{\min} . Then, the eigenvector corresponding to I_j^{\min} gives the orientation of the long axis of the chain.

In order to calculate the total phase lag, α , we averaged the chain phase lag distribution weighted by the chain size

$$\alpha = \frac{\sum_j N_j \alpha_j}{N_a}, \quad [11]$$

where the sum is done for j with $N_j > 1$. The reason for this choice is that, qualitatively speaking, the contribution of each chain to the anisotropy of the total scattering pattern is larger the larger the chain size, therefore, one should expect that long chains should contribute comparatively more to the average phase lag than short chains.

The computations described so far consider straight chains and, obviously do not take into account the shape of the clusters. However, previous videomicroscopy results show that very long chains deviate significantly from straight lines, and, moreover, at high frequencies small clusters less anisotropic may appear. To assess the effect of these chain form anomalies in our simulations results, we calculated the same quantities, L , N_a , and α using a weight function that takes into account the shape of the cluster. Actually we used $W_j = N_j s_j$, where s_j is a shape factor with value 1 for the case of a straight chain, and 0 for a symmetric cluster

$$s_j = \frac{(I_j^{\max})^{1/2} - (I_j^{\min})^{1/2}}{(I_j^{\max})^{1/2} + (I_j^{\min})^{1/2}}. \quad [12]$$

We did not observe appreciable changes in the simulations results using this shape correction. Therefore, we present here the results corresponding to the case without the shape factor.

3.2.3. Simulation Results. In Fig. 7 we plot the particle positions in the (X, Y) plane for different dimensionless frequencies at an arbitrary time. The field rotates in the counter clockwise direction. Several qualitative observations can be made on Fig. 7. First, the size of the structures becomes smaller as the rotational frequency increases. Second, at low Ma (see Fig. 7a), the deformation of the chains is larger the longer the chain is, and the shape of the deformed chain is qualitatively similar to the one predicted by Martin *et al.* (20) for the closely related case of electrorheological suspensions under a simple shear flow. Third, at high Ma (see Fig. 7d), the tendency to form chains aligned with the field is not clearly apparent, and more isotropic clusters appear to be preferred; moreover, a higher number of isolated particles appears.

Some of these observations can be made more quantitative by studying the average chain length. The dimensionless average chain length, L , versus Ma in a log-log plot is shown in Fig. 8. The average chain length follows a power law behavior with an exponent approximately equal to -0.45 . This behavior agrees well with the one predicted by the chain model (20, 21) developed for the case of electrorheological fluids subject to a simple steady shear flow, which predicts a power law behavior with exponent $-1/2$.

Figure 9 shows the total number of aggregated particles, N_a , versus Ma in a log-log plot. Two different regions appears, in agreement with the experimental dichroism. First, there is a plateau zone at low Ma , in which N_a varies very little with Ma . Second, a strongly decreasing response appears for $Ma \geq 1$, with an apparent exponent close to -1 , although the region in which this power law behavior could be studied in the simulations is rather small.

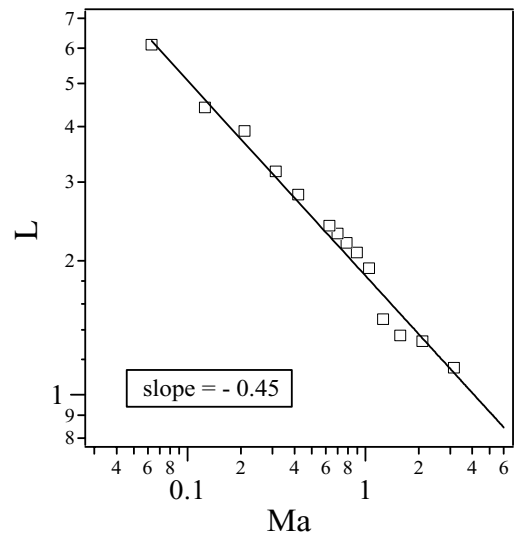


FIG. 8. Dimensionless average chain length, L , versus dimensionless rotational frequency, $\Omega \equiv Ma$, in a log-log plot (symbols). The power law fit (solid line) gives an exponent equal to -0.44 ± 0.02 . Calculations for suspension d-M1-180/12 (82.5% glycerol, $\phi = 0.016$).

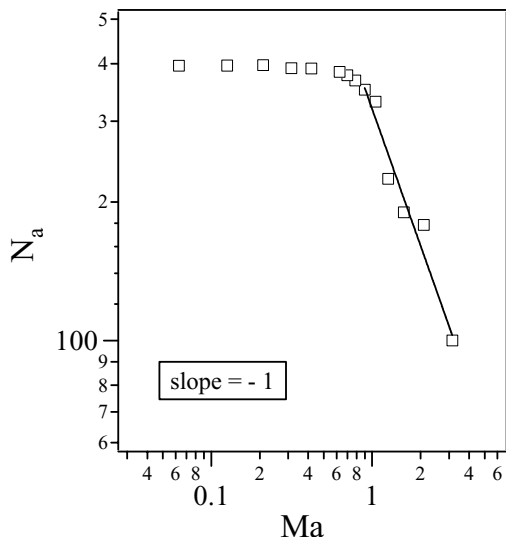


FIG. 9. Total number of aggregated particles, N_a , versus dimensionless rotational frequency, $\Omega \equiv Ma$, in a log-log plot (symbols). The power law fit (solid line) for $Ma > Ma_c$ gives an exponent equal to -1.0 ± 0.1 . Calculations for suspension d-M1-180/12 (82.5% glycerol, $\phi = 0.016$).

The picture that emerges from these results is the following: the average chain length decreases monotonously with Ma ; however, at low Ma , this decrease in length does not show up in the number of aggregated particles, because almost all particles are aggregated although the chains that are stable become shorter as Ma increases. At $Ma_c \simeq 1$, the average chain length is approximately 2 (see Fig. 8), which is, obviously, the smallest chain that can be formed. Therefore, at $Ma > 1$, chains formed

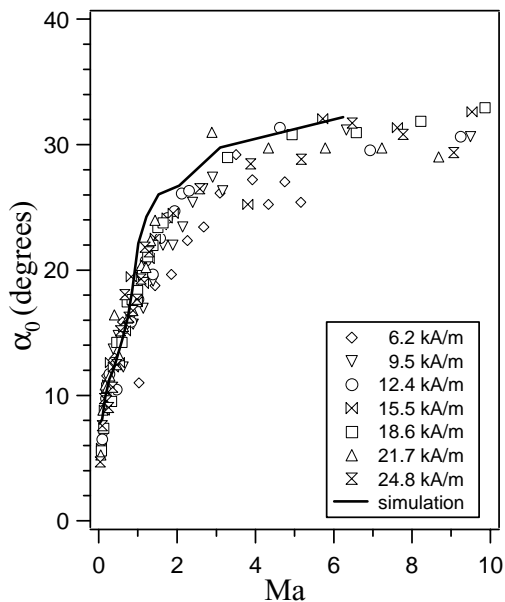


FIG. 10. Experimental steady phase lag, α_0 , (symbols) and phase lag obtained from the simulations (solid line) as a function of Ma . Measurements for suspension d-M1-180/12 (82.5% glycerol, $\phi = 0.016$).

by two particles become unstable, and, consequently, the total number of aggregated particles starts to decrease. These results also confirm the conjecture that the scattering dichroism represents well the total number of aggregated particles in the measurement volume.

A more specific comparison between the information obtained from the scattering dichroism measurements and the simulation results can be done in terms of the phase lag. In Fig. 10, we compare the experimental values of the steady phase lag, α_0 , (symbols) with the values obtained from the simulation using Eq. [11] (solid line). The agreement is rather good, although the values obtained in the simulations consistently appear in the upper range of the experimental values.

4. CONCLUSIONS

In this work we used scattering dichroism to analyze the interplay of the magnetic and viscous forces in the dynamics of magnetorheological suspensions under rotating magnetic fields. In these suspensions, dichroism arises from the formation of optically anisotropic chains upon imposition of the magnetic field. Under rotating fields, two different behaviors for the dichroism and the phase lag are found above or below a cross-over frequency. At low frequencies, the chains rotate with the field, yielding a dichroism that is independent of frequency, but with a constant phase lag that increases with frequency. At high frequencies, the dichroism decreases roughly as f^{-1} , and the phase lag increases more slowly. We obtained a good collapse of the dichroism and the phase angle assuming a linear dependence of the cross-over frequency both with the square of the magnetization and with the inverse of the viscosity. This means that the Mason number (ratio of viscous to magnetic forces) is the relevant dimensionless parameter for the problem. The experimental results show that the cross-over value of Ma is $Ma_c \simeq 1$. This fact implies that the cross-over appears when the chains formed by two particles lose mechanical stability (20, 21) because hydrodynamic friction forces overcome magnetic dipolar attraction.

In the parameter range here studied, athermal simulations incorporating Stokes friction and dipole-dipole magnetic interaction are able to accurately reproduce the experimental results. According to the simulations, the average length of the chain-like structures decreases when increasing the rotational frequency, scaling as the inverse square root of the Mason number. Furthermore, the simulations reproduce two different behaviors above and below Ma_c for the total number of aggregated particles, N_a , and the phase lag, α , in agreement with the experiments.

ACKNOWLEDGMENTS

This work was partially supported by the Lai Family Grant, and MEC Grants PB96-0148 and BFM2000-0019. S.M. was supported by MEC Grant PB96-0148. We gratefully acknowledge A. P. Gast and J. E. Martin for fruitful discussions.

REFERENCES

1. The form dichroism measures the difference between the absorption of the incident light with polarization parallel and perpendicular to the long axis of the scattering objects. The form birefringence arises from a spatially anisotropic arrangement of domains with different refractive indexes.
2. van de Hulst, H. C., "Light Scattering by Small Particles," Dover Publications, New York, 1981.
3. Melle, S., Fuller, G. G., and Rubio, M. A., *Phys. Rev. E* **61**, 4111 (2000).
4. Melle, S., Rubio, M. A., and Fuller, G. G., *Phys. Rev. Lett.* **87**, 115,501 (2001).
5. Helgesen, G., Pieranski, P., and Skjeltorp, A. T., *Phys. Rev. Lett.* **64**, 1425 (1990); Helgesen, G., Pieranski, P., and Skjeltorp, A. T., *Phys. Rev. A* **42**, 7271 (1990).
6. Migler, K. B., and Meyer, R. B., *Phys. Rev. Lett.* **66**, 1485 (1991).
7. Zheng, C., and Meyer, R. B., *Phys. Rev. E* **55**, 2882 (1997).
8. Melle, S., Calderón, O. G., Rubio, M. A., and Fuller, G. G., *J. Non-Newtonian Fluid Mech.*, in press.
9. Similar behavior was previously found for magnetic droplets in emulsions under rotating fields in O. Sandre *et al.*, *Phys. Rev. E* **59**, 1736 (1999).
10. Mason number was first introduced in literature for ER fluids under steady shear. See A. P. Gast and C. F. Zukoski, *Adv. Colloid Interface Sci.* **30**, 153 (1989).
11. Volkova, O., Cutillas, S., and Bossis, G., *Phys. Rev. Lett.* **82**, 233 (1999).
12. Martin, J. E., *Phys. Rev. E* **63**, 11,406 (2001).
13. Fuller, G. G., "Optical Rheometry in Complex Fluids," Oxford University Press, London, 1995.
14. Jones, T. B., "Electromechanics of Particles," Cambridge, Cambridge, UK, 1995.
15. Kashevsky, B. E., and Novokova, A. L., *Magnetohydrodynamics* **25**, 304 (1989).
16. Martin, J. E., Anderson, R. A., and Tigges, C. P., *J. Chem. Phys.* **108**, 3765 (1998).
17. Mohebi, M., Jamasbi, N., and Liu, Jing, *Phys. Rev. E* **54**, 5407 (1996).
18. Klingenberg, D. J., van Swol, F., and Zukovski, C. F., *J. Chem. Phys.* **91**, 7888 (1989).
19. Larson, R. G., "The Structure and Rheology of Complex Fluids," Oxford University Press, New York, 1999.
20. Martin, J. E., and Anderson, R. A., *J. Chem. Phys.* **104**, 4814 (1996).
21. The same behavior $L \propto \text{Ma}^{-1/2}$ is also obtained for a chain model in the case of rotating magnetic fields: S. Melle and J. E. Martin (to be published).